PHOTONICS Research

Soliton and bound-state soliton mode-locked fiber laser based on a MoS_2/fluorine mica Langmuir–Blodgett film saturable absorber

Ruidong Lü,[1] Yonggang Wang,[1,*] Jiang Wang,[1] Wei Ren,[2] Lu Li,[2] Sicong Liu,[1] Zhendong Chen,[1] Yongfang Li,[1] Hongying Wang,[3] and Fuxing Fu[3]

[1]School of Physics and Information Technology, Shaanxi Normal University, Xi'an 710119, China
[2]School of Science, Xi'an Institute of Posts and Telecommunications, Xi'an 710121, China
[3]Key Laboratory for Surface Engineering and Remanufacturing of Shaanxi Province, Xi'an University, Xi'an 710065, China
*Corresponding author: chinawygxjw@snnu.edu.cn

Received 4 September 2018; revised 7 December 2018; accepted 27 January 2019; posted 29 January 2019 (Doc. ID 345011); published 14 March 2019

In this article, we report on an experimentally generated soliton and bound-state soliton passively mode-locked erbium-doped fiber laser by incorporating a saturable absorber (SA) made of MoS_2/fluorine mica (FM) that was fabricated with the Langmuir–Blodgett (LB) method. The FM substrate is 20 μm thick and easy to bend or cut, like a polymer. However, it has a higher damage threshold and a better thermal dissipation than polymers. In addition, the LB method can be used to fabricate a thin film with good uniformity. In this study, the modulation depth, saturable intensity, and unsaturated loss of the SA are measured as 5.9%, 57.69 MW/cm^2, and 13.4%, respectively. Based on the SA, a soliton mode-locked laser is achieved. The pulse duration, repetition rate, and signal-to-noise ratio are 581 fs, 15.67 MHz, and 65 dB, respectively. By adjusting the polarization controller and pump power, we obtain a bound-state soliton mode-locked pulse. The temporal interval between the two solitons forming the bound-state pulse is 2.7 ps. The repetition rate of the bound-state pulses is proportional to the pump power. The maximum repetition rate is 517 MHz, corresponding to the 33rd harmonic of the fundamental repetition rate. The results indicate that the MoS_2/FM LB film absorber is a promising photonic device in ultrafast fiber lasers.

https://doi.org/10.1364/PRJ.7.000431

1. INTRODUCTION

Passively mode-locked fiber lasers have many widespread applications in the field of nonlinear optics, optical fiber communication, material processing, and optical sensing because of their good stability, high beam quality, and compact design [1–3]. In recent decades, the generation of passively mode-locked pulse lasers mainly depended on nonlinear optical loop mirrors (NOLMs) [4], nonlinear polarization rotation (NPR) [5], and saturable absorbers (SAs) [6,7]. However, the NOLM and NPR techniques are susceptible to the surrounding environment and usually need a relatively high pump power for the mode-locked operation, thus limiting their practical applications [8,9]. As a type of SA, semiconductor SA mirrors (SESAMs) are considered as practical absorbers and have been widely used in commercial laser systems [10,11]. However, SESAMs have some disadvantages such as high cost, a complex fabrication process, narrow waveband, and long response time [12]. Two-dimensional (2D) materials such as graphene [13,14], topologic insulators (TIs) [15,16], transition-metal dichalcogenides (TMDs) [17–23], black phosphorus [24,25], perovskite [26], MXene [27], and antimonene [28] have great application potential in nonlinear optics and ultrafast photonics. Compared with SESAMs, 2D nonlinear materials have some advantages, such as broadband saturable absorption, ultrafast recovery time, and a high nonlinear optical absorption coefficient.

Recent reports have shown that the band gap width of TMDs can be changed by manipulating their thickness or introducing atomic defects, thus obtaining a series of excellent properties [29–31]. Molybdenum disulfide (MoS_2) is an atypical TMD material. Bulk MoS_2 is an indirect semiconductor with a band gap of 1.29 eV, whereas monolayer MoS_2 is a direct semiconductor with a band gap of 1.8 eV [32,33]. Few-layer MoS_2 with semiconducting properties can be excited by absorbing one photon with a higher energy than the band gap. At high excitation intensity, electrons in the valence band are transferred to fill the conduction band [34]. Similar to the zero-band gap of graphene and the surface state of TIs, few-layer MoS_2 of the semiconductor phase can also exhibit broadband saturable absorption with the help of the Pauli

blocking effect. Moreover, the study shows that the intraband transition of stimulated free carriers is approximately 30 fs, and the lifetime of interband transition is a picosecond time scale of MoS_2, and it has a better saturation absorption response than graphene [34,35]. In fiber lasers, TMD nanosolutions can be deposited at the fiber ends, fused taper fibers, and D-type fibers, or directly embedded in photonic crystal fibers. Among them, the van der Waals force of fiber end deposition method is very weak, causing loose contact between the SA and fiber surface. The fabrication processes based on evanescent field SAs are very complex and fragile, causing additional light loss and fabrication cost [36]. The polymer film [37–39] has the advantages of low cost, flexibility, and controllability, and it is more favorable to the preparation of SAs, but its damage threshold is very low [40]. In addition, SA films fabricated by the drop-coating or spin-coating method have a rough surface and uneven material distribution [41,42]. This will introduce extra optical scattering losses into the laser cavity and reduce the performance of the laser.

Here, to the best of our knowledge, a new Langmuir–Blodgett (LB) method is used to fabricate a broadband absorber, which is combined with an inorganic matrix fluorine mica (FM) sheet and MoS_2, to produce a high-performance SA device. The LB technique disperses molecules of hydrophilic head groups and hydrophobic tail groups on the water surface. A horizontal pressure is applied on the surface of the water so that the molecules are closely arranged on the water surface to form a monolayer or few-layer insoluble films. By controlling the surface pressure of the solution and the film-forming speed, the quality of the films can be effectively improved [43–45]. Although the magnetron sputtering deposition method and the chemical vapor deposition method are excellent methods to improve the uniformity of large-area coating [46,47], with these methods, it is not easy to adjust the thickness of the absorber as freely as the LB method does. In comparison, the LB method has low cost and can be prepared under normal temperature and pressure conditions to avoid damage to nanomaterials and the membrane structure. Therefore, the LB method is widely used in material science, optics, electrochemistry, and bio-bionics as one of the main methods to prepare nanometer thin films [48,49]. FM is an ideal substrate material with 12 times the hardness and 6–8 times the melting point of polyvinyl alcohol (PVA). It is not easy to break owing to good elasticity. Because of its resistance to high temperatures and good light transmission, the damage threshold is much greater than in organic films [41]. Excellent flatness will not cause deviation when FM is inserted into a fiber laser. In this study, MoS_2 is used as the SA material and transferred onto single-layer FM via the LB technique. The modulation depth (MD) and unsaturated loss (UL) of MoS_2/FM are 5.9% and 13.4%, respectively. Using the SA in an erbium-doped fiber (EDF) laser, we obtain a mode-locked pulse with the pulse duration of 581 fs and an average power of 9.6 mW. By adjusting the pump power, we obtain the bound-state soliton mode locking. In the cavity, the time interval between the two solitons forming the bound-state pulse is 2.7 ps. The bound-state pulse is evenly distributed, and the repetition rate increases with the pump power. The maximum repetition rate is 517 MHz, 33 times the fundamental repetition rate.

2. PREPARATION AND CHARACTERIZATION OF MoS_2/FM LB FILMS

The MoS_2 nanosheet solution is prepared by using the liquid-phase stripping method. First, MoS_2 powders are dispersed in deionized water and treated for 12 hours with an ultrasonic cleaner to obtain a MoS_2 solution with a concentration of 1 mg/mL. Then, the MoS_2 solution is mixed with methanol at a volume ratio of 1:4. Chloroform is added to the mixture to increase the diffusion of nanometer solution on the water subphase. Hydrophilic treatment is carried out for FM with a size of 1 cm × 1 cm and a thickness of 20 μm.

The fabrication process of SA devices is shown in Fig. 1(a). FM is vertically inserted into the double-barrier Langmuir

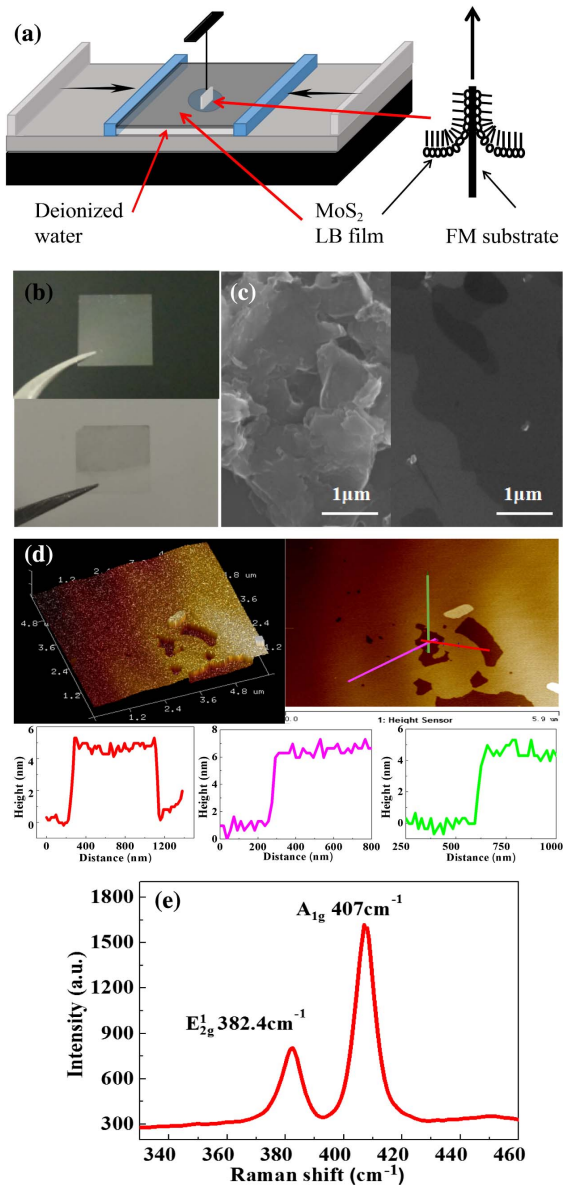

Fig. 1. (a) Fabrication process of SA devices. (b) Macroscopic images of FM and MoS_2/FM. (c) SEM image of a MoS_2 SA by the spin-coating and LB methods at the same resolutions. (d) 3D and plane AFM image and the AFM height profile diagram of few-layer MoS_2. (e) Raman spectrum of the MoS_2 SA.

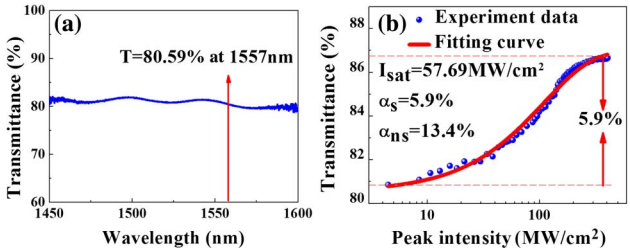

Fig. 2. (a) Linear transmittance measured in the spectral range from 1450 to 1600 nm. (b) Nonlinear saturable absorption of the MoS_2/FM LB film.

trough of half-filled water subphases. Then, the MoS_2–methanol–chloroform solution is slowly dropped into the aqueous subphase at a rate of 0.1 mL/min for 30 min. A pair of moving barriers is used to compress the SA membrane until the surface pressure reaches 22 mN/m. Then, FM keeps rising at a rate of 0.8 mm/min, so that the floating layer is uniformly adsorbed on the FM surface. Finally, the SA device is annealed for 2 hours in a drying oven maintained at 60°C. Figure 1(b) shows macroscopic images of FM and MoS_2/FM. The upper part of Fig. 1(b) shows pure FM without an SA. The lower part clearly shows a thick layer of the SA on the FM. To verify the surface quality of the MoS_2 LB film, the scanning electron microscope (SEM) morphology of MoS_2/FM is measured. As presented in Fig. 1(c), the left and right parts show that the MoS_2/FM SA is obtained by spin-coating and the LB method, respectively. In the left part, the agglomeration of fine particles is observed on the surface of the film fabricated by the spin-coating method. In the right part, the surface of the film fabricated by the LB method is uniform and compact. An atomic force microscope (AFM) is used to characterize the thickness of the MoS_2/FM LB film, as shown in Fig. 1(d). The three-dimensional (3D) surface topography results show that the MoS_2 nanosheets are densely distributed in a large area of 6 μm × 6 μm. The average thickness of LB films is ~4 nm in three different directions, indicating that the thickness of the MoS_2 LB film is relatively uniform. To study the Raman shift characteristics of the MoS_2/FM LB film, the Raman spectrum of the MoS_2 SA is measured by a 532 nm laser. As shown in Fig. 1(e), two characteristic peaks are located at 382.4 cm^{-1} and 407 cm^{-1}, respectively. Generally, the thickness of the sample is estimated from the frequency difference between the two main modes. Here, the frequency difference between the two characteristic peaks is 24.6 cm^{-1}. Compared with the reported MoS_2 Raman spectrum, it is proved that the thickness of our LB film is 4–5 layers [50].

As shown in Fig. 2(a), the linear transmission spectrum of the MoS_2/FM SA is measured in the range from 1450 to 1600 nm. At the wavelength of 1557 nm, the transmittance of MoS_2/FM is 80.59%. Finally, the nonlinear saturable absorption property of MoS_2/FM is studied. A home-made femtosecond laser with a central wavelength of 1562 nm, repetition rate of 24.93 MHz, and pulse width of 500 fs is used as the test source. The laser is divided into two beams with a 50:50 coupler, one beam for the power-dependent transmission measurement of the SA device and the other for reference. The measured results are fitted by the function $T = A\exp[-\Delta T/(1 + I/I_{sat})]$. Here, A is the normalization constant, ΔT is the MD, I is the incident intensity, and I_{sat} is the saturation intensity. The results are shown in Fig. 2(b). The MD, I_{sat}, and UL of MoS_2/FM are 5.9%, 57.69 MW/cm^2, and 13.4%, respectively.

Table 1 shows a comparison of typical TMD SA mode-locked fiber lasers. The results show that MoS_2/FM LB thin films have a lower UL value and a higher average output power compared with other preparation methods. This indicates that the scattering loss and absorption loss of MoS_2/FM LB films are relatively low because the preparation of the SA device introduced fewer impurities, and the surface is highly uniform.

3. EXPERIMENTAL SETUP

The MoS_2/FM SA is applied in an erbium-doped all-fiber laser. Figure 3 shows the schematic diagram of the experimental device. A laser diode (LD) with a wavelength of 976 nm is used as the pump source, and the maximum output power is 500 mW. A piece of 1.8 m EDF is used as the gain medium of the laser. The pump light is transmitted to the EDF through a 980/1550 nm wavelength division multiplexer (WDM) coupler. A polarization insensitive isolator (PI-ISO) is connected to the EDF to ensure unidirectional operation and eliminate reflection in the laser cavity. A polarization controller (PC) is used to adjust the cavity polarization to optimize the laser mode-locking performance. A fused fiber optical coupler (OC) is used to extract 10% of the energy from the laser cavity.

With the exception of EDF, other fibers and pigtails of the components are single mode fiber-28 (SMF-28) in the cavity. The total cavity length of the laser is ~13.2 m. The group velocity dispersions of the SMF-28 and the EDF are –23.9 ps^2/km and 42 ps^2/km at 1560 nm, respectively; thus,

Table 1. Comparison of Nonlinear Parameters and Corresponding Mode-Locked EDF Lasers Based on a TMD SA

Materials	SA type	Layer	MD (%)	UL (%)	λ (nm)	τ (fs)	P_{ave} (mW)	Reference
WS_2	PVA	—	2.9	30.9	1572	595	—	[17]
WS_2	Taper	7–9	0.5	65.0	1563	563	2.8	[18]
WSe_2	Polymethylmethacrylate-side-polished fiber (PMMA-SPF)	1–3	54.5	—	1556	477	—	[19]
$MoSe_2$	PVA	2–3	0.6	3.5	1558	1450	0.4	[20]
MoS_2	PVA	5–6	2.7	44.2	1556	606	5.9	[21]
MoS_2	Fiber facet	4–5	35.4	34.1	1569	1280	5.1	[22]
MoS_2	PMMA-SPF	<10	>2.5	<70.0	1568	637	—	[23]
MoS_2	FM LB film	4–5	5.9	13.4	1557	581	9.6	This study

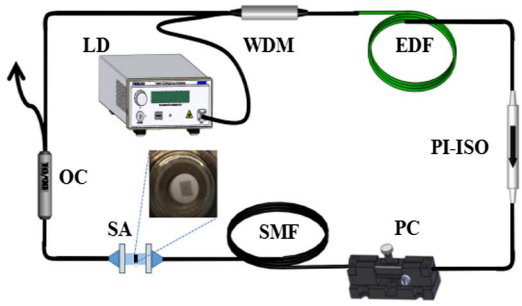

Fig. 3. Configuration of a passively mode-locked EDF laser.

the net cavity dispersion was estimated as −0.197 ps^2. The MoS_2/FM SA device is spliced inside the laser cavity to start the mode-locking operation. The output laser characteristics are monitored with an optical spectrum analyzer (Yokogawa AQ6370D), a 1G digital oscilloscope (Rohde & Schwarz RTO1014) equipped with a home-made 5G photodetector, a radio frequency (RF) analyzer (Rohde & Schwarz FSV 13), and an optical autocorrelator (APE Pulsecheck).

4. RESULTS AND DISCUSSION

In the experiment, continuous wave (CW) emission occurs when the pump power increases to 22 mW. The mode-locked operation appeared at the pump power of 37 mW and was maintained until 500 mW, during which multiple pulses were not observed. The performance of the mode-locked fiber laser is shown in Fig. 4 at the pump power of 450 mW. Figure 4(a) shows a typical mode-locked spectrum. The central wavelength and the 3 dB bandwidth are 1557.2 nm and 4.8 nm, respectively. As shown in Fig. 4(b), the autocorrelation trace has a full width at half maximum of 895 fs. By fitting the autocorrelation trace with a sech^2 function, the pulse duration is estimated to be 581 fs. The time-bandwidth product is 0.345, indicating that the mode-locked pulse is slightly chirped. Furthermore, an autocorrelation trace with a broad scanning range of 80 ps is illustrated in Fig. 4(b). It confirms the singe pulse operation under the highest pump power. Figure 4(c) shows the oscilloscope trace of a mode-locked pulse train. The pulse train shows a relatively uniform intensity with a pulse interval of 63.83 ns, corresponding to the round-trip time within the cavity. Figure 4(d) shows the radio frequency spectra of the generated pulse train. A strong signal peak exhibits the cavity fundamental repetition rate of 15.67 MHz, corresponding to a laser cavity length of 13.2 m. The signal-to-noise ratio measured at 1 kHz resolution bandwidth is 65 dB, indicating that the mode-locking operation is very stable. The 500-MHz-span RF spectrum in the inset suggests that the fiber laser operates well in the continuous mode-locking state.

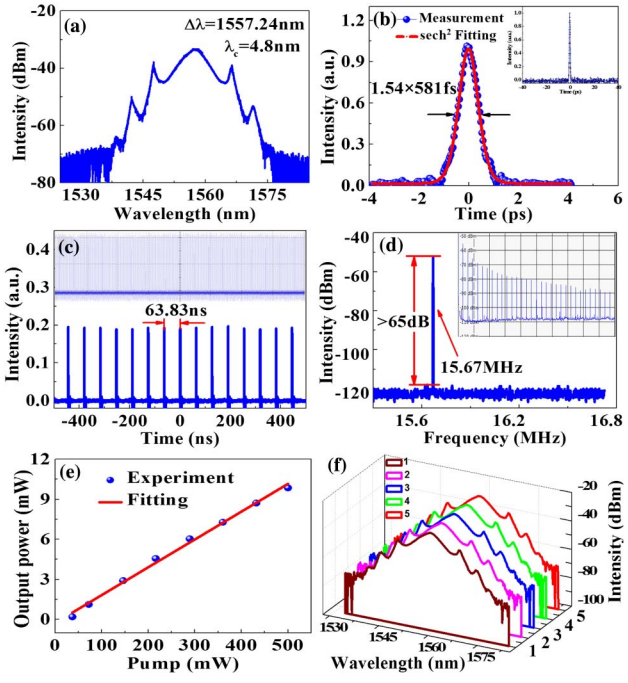

Fig. 4. Characterization of the soliton mode-locked fiber laser: (a) optical spectrum, (b) autocorrelation trace, (c) oscilloscope trace, (d) RF spectrum, and (e) the relationship between the output power and pump power of soliton mode locking. (f) Long-term optical spectrum measured for five days.

Figure 4(e) shows that the average output power linearly increases with the pump power. At the maximum pump power of 500 mW, the average output power is 9.6 mW, corresponding to the pulse energy of 0.613 nJ. Further improvement of the system efficiency is possible using an output coupler with a large split ratio and further optimizing the cavity parameters [51]. In addition, the use of high-gain and large-mode area fibers is also a good way to improve the output efficiency. To evaluate the long-term stability of a mode-locked fiber laser, the experiments were performed for five days. The optical spectrum of the mode-locked fiber laser was recorded every day, as shown in Fig. 4(f). No significant degradation was observed, indicating that the SA was not damaged after days of continuous high-power operation. This shows that the MoS_2/FM LB film SA has a high laser damage threshold.

By changing the pump power to 307 mW and adjusting the polarization state, the laser turns into the bound-state soliton mode locking. As shown in Fig. 5(a), the side-band of the output spectrum verifies the soliton mode-locked state of the laser. The spectrum shows a regular modulation with a period of 3 nm, which is an important feature of the bound-state soliton. Figure 5(b) shows a typical result of the autocorrelation trajectory, exhibiting three peaks with an intensity ratio of 1:2:1. This indicates that the two solitons of the bound-state pulse have the same intensity [52]. The soliton pulse interval is 2.7 ps, 3.4 times the pulse width of 805 fs. Such a short time

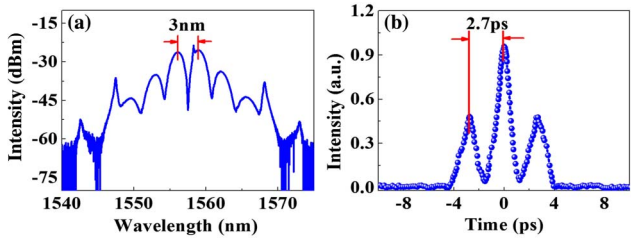

Fig. 5. Experimental results of a bound-state soliton mode-locked fiber laser. (a) Optical spectrum and (b) autocorrelation trace.

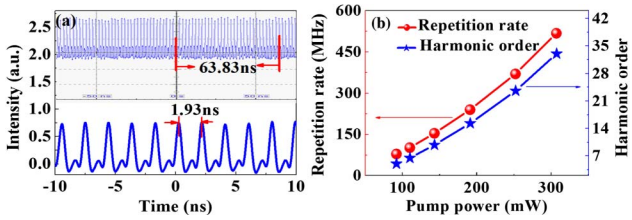

Fig. 6. (a) Bound-state pulse oscilloscope trace with a pump power of 307 mW. (b) Repetition rate and harmonic number under a different pump power.

interval of bound-state solitons indicates that the direct interaction between two solitons originates from the attractive or repulsive force exerted on each soliton [53]. Here, the spectral modulation interfringe is inversely proportional to the temporal separation of pulses $\Delta\nu = 1/\tau$ [54]. The period of the spectral modulation is 3 nm ($\Delta\nu = 371.24$ GHz). The calculated bound soliton separation based on the Fourier analysis (2.69 ps) corresponds well to the experimental observation from the autocorrelation trace (2.7 ps).

Figure 6(a) shows the pulse sequence with the pump power of 307 mW. Within the interval of 63.83 ns, 33 bound-state pulses are observed, and the interval is 1.93 ns, the 33rd harmonics of the fundamental repetition rate. Because each bound-state pulse consists of two solitons, 66 solitons propagate in the fiber laser. This formation process describes that the solitons form a bound-state pulse, and then the bound-state pulses are rearranged and regularly distributed in the laser cavity [55,56]. Based on the above results, we believe that the fiber laser operates at the bound-state harmonic mode locking.

In the experiment, we found that the repetition rate of bound-state pulses decreases with the pump power decrease. The repetition rate and harmonic number are shown in Fig. 6(b). From 517.8 MHz at the pump power of 307 mW to 78.8 MHz at the pump power of 92 mW, the corresponding harmonic number decreases from 33 to 5.

Finally, the MoS_2/FM SA device is removed from the laser cavity to verify whether the mode-locking formation is caused only by the SA. In this case, no mode-locking is observed, even though the pump power is changed from zero to maximum, and the PC is tuned over the entire range. By inserting MoS_2/FM in the fiber laser, the mode-locking operation can be achieved again. Therefore, it can be concluded that the mode-locking operation is completely caused by the SA instead of other components. Based on the experimental observation, we believe that the MoS_2/FM LB film has nonlinear saturable absorption properties, and thus it can be used as a mode-locking device for ultrafast fiber lasers.

5. CONCLUSION

In summary, a few layers of MoS_2 LB films were prepared on an FM substrate. The surface morphology and nonlinear properties of the film were tested. The MoS_2/FM LB film SA exhibited a uniform surface distribution, small UL, and a high damage threshold. Using an SA in a fiber laser, stable fundamental mode locking with a pulse width of 581 fs and the maximum power of 9.6 mW was achieved. By adjusting the PC, bound-state soliton mode locking was obtained. The time interval between the two solitons was 2.7 ps. The repetition rate of the bound-state pulse increased with the pump power, and the maximum repetition rate was 517 MHz. The results show that the MoS_2/FM LB film has potential practical applications in ultrafast photonics and optoelectronics.

Funding. Central University Special Fund Basic Research and Operating Expenses (GK201702005); Natural Science Foundation of Shaanxi Province (2017JM6091); National Natural Science Foundation of China (NSFC) (61705183); Fundamental Research Funds for the Central Universities (2017TS011).

REFERENCES

1. U. Keller, "Recent developments in compact ultrafast lasers," Nature **424**, 831–838 (2003).
2. B. Oktem, C. Ulgudur, and F. O. Ilday, "Soliton-similariton fibre laser," Nat. Photonics **4**, 307–311 (2010).
3. Y. D. Cui, D. D. Han, X. K. Yao, and Z. P. Sun, "Distributed ultrafast fibre laser," Sci. Rep. **5**, 9101 (2015).
4. L. Yun and X. M. Liu, "Generation and propagation of bound-state pulses in a passively mode-locked figure-eight laser," IEEE Photon. J. **4**, 512–519 (2012).
5. A. P. Luo, Z. C. Luo, W. C. Xu, V. V. Dvoyrin, V. M. Mashinsky, and E. M. Dianov, "Tunable and switchable dual-wavelength passively mode-locked Bi-doped all-fiber ring laser based on nonlinear polarization rotation," Laser Phys. Lett. **8**, 601–605 (2011).
6. L. E. Nelson, D. J. Jones, K. Tamura, H. A. Haus, and E. P. Ippen, "Ultrashort-pulse fiber ring lasers," Appl. Phys. B **65**, 277–294 (1997).
7. I. N. Duling, "All-fiber ring soliton laser mode locked with a nonlinear mirror," Opt. Lett. **16**, 539–541 (1991).
8. Q. L. Bao, H. Zhang, Y. Wang, Z. H. Ni, Y. L. Yan, Z. X. Shen, K. P. Loh, and D. Y. Tang, "Atomic-layer graphene as a saturable absorber for ultrafast pulsed lasers," Adv. Funct. Mater. **19**, 3077–3083 (2009).
9. H. Zhang, D. Y. Tang, L. M. Zhao, Q. L. Bao, and K. P. Loh, "Large energy mode locking of an erbium-doped fiber laser with atomic layer graphene," Opt. Express **17**, 17630–17635 (2009).
10. U. Keller, K. J. Weingarten, F. X. Kartner, D. Kopf, B. Braun, I. D. Jung, R. Fluck, C. Honninger, N. Matuschek, and J. Aus der Au, "Semiconductor saturable absorber mirrors (SESAM's) for femtosecond to nanosecond pulse generation in solid-state lasers," IEEE J. Sel. Top. Quantum Electron. **2**, 435–453 (1996).
11. A. A. Lagatsky, F. Fusari, S. Calvez, S. V. Kurilchik, V. E. Kisel, N. V. Kuleshov, M. D. Dawson, C. T. A. Brown, and W. Sibbett, "Femtosecond pulse operation of a Tm, Ho-codoped crystalline laser near 2 micron," Opt. Lett. **35**, 172–174 (2010).
12. P. G. Yan, R. Y. Lin, S. C. Ruan, A. J. Liu, H. Chen, Y. Q. Zheng, S. F. Chen, C. Y. Guo, and J. G. Hu, "A practical topological insulator saturable absorber for mode-locked fiber laser," Sci. Rep. **5**, 8690 (2015).
13. T. Hasan, Z. P. Sun, F. Q. Wang, F. Bonaccorso, P. H. Tan, A. G. Rozhin, and A. C. Ferrari, "Nanotube-polymer composites for ultrafast photonics," Adv. Mater. **21**, 3874–3899 (2009).
14. J. Sotor, I. Pasternak, A. Krajewska, W. Strupinski, and G. Sobon, "Sub-90 fs a stretched-pulse mode-locked fiber laser based on a graphene saturable absorber," Opt. Express **23**, 27503–27508 (2015).
15. C. J. Zhao, H. Zhang, X. Qi, Y. Chen, Z. T. Wang, S. C. Wen, and D. Y. Tang, "Ultra-short pulse generation by a topological insulator based saturable absorber," Appl. Phys. Lett. **101**, 211106 (2012).
16. H. H. Shao, Y. M. Liu, X. Y. Zhou, and G. H. Zhou, "Electron states scattering off line edges on the surface of topological insulator," Chin. Phys. B **23**, 107304 (2014).
17. K. Wu, X. Zhang, J. Wang, X. Li, and J. Chen, "WS_2 as a saturable absorber for ultrafast photonic applications of mode-locked and Q-switched lasers," Opt. Express **23**, 11453–11461 (2015).
18. R. Khazaeinezhad, S. H. Kassani, H. Jeong, K. J. Park, B. Y. Kim, D. Yeom, and K. Oh, "Ultrafast pulsed all-fiber laser based on tapered

fiber enclosed by few-layer WS_2 nano-sheets," IEEE Photon. Technol. Lett. **27**, 1581–1584 (2015).
19. J. D. Yin, J. R. Li, H. Chen, J. T. Wang, P. G. Yan, M. L. Liu, W. J. Liu, W. Lu, Z. H. Xu, W. F. Zhang, J. Z. Wang, Z. P. Sun, and S. C. Ruan, "Large-area highly crystalline WSe_2 atomic layers for ultrafast pulsed lasers," Opt. Express **25**, 30020–30031 (2017).
20. Z. Q. Luo, Y. Y. Li, M. Zhong, Y. Z. Huang, X. J. Wan, J. Peng, and J. Weng, "Nonlinear optical absorption of few-layer molybdenum diselenide ($MoSe_2$) for passively mode-locked soliton fiber laser," Photon. Res. **3**, A79–A86 (2015).
21. K. Wu, X. Y. Zhang, J. Wang, and J. P. Chen, "463-MHz fundamental mode-locked fiber laser based on few-layer MoS_2 saturable absorber," Opt. Lett. **40**, 1374–1377 (2015).
22. H. D. Xia, H. P. Li, C. Y. Lan, C. Li, X. X. Zhang, S. J. Zhang, and Y. Liu, "Ultrafast erbium-doped fiber laser mode-locked by a CVD-grown molybdenum disulfide (MoS_2) saturable absorber," Opt. Express **22**, 17341–17348 (2014).
23. R. Khazaeizhad, S. H. Kassani, H. Jeong, D. Yeom, and K. Oh, "Mode-locking of Er-doped fiber laser using a multilayer MoS_2 thin film as a saturable absorber in both anomalous and normal dispersion regimes," Opt. Express **22**, 23732–23742 (2014).
24. Z. C. Luo, M. Liu, Z. N. Guo, X. F. Jiang, A. P. Luo, C. J. Zhao, X. F. Yu, W. C. Xu, and H. Zhang, "Microfiber-based few-layer black phosphorus saturable absorber for ultra-fast fiber laser," Opt. Express **23**, 20030–20039 (2015).
25. S. C. Liu, Y. N. Zhang, L. Li, Y. G. Wang, R. D. Lv, X. Wang, Z. D. Chen, and L. L. Wei, "Er-doped *Q*-switched fiber laser with black phosphorus/polymethyl methacrylate saturable absorber," Appl. Opt. **57**, 1292–1295 (2018).
26. G. B. Jiang, L. L. Miao, J. Yi, B. Huang, W. Peng, Y. H. Zou, H. H. Huang, W. Hu, C. J. Zhao, and S. C. Wen, "Ultrafast pulse generation from erbium-doped fiber laser modulated by hybrid organic-inorganic halide perovskites," Appl. Phy. Lett. **110**, 161111 (2017).
27. X. T. Jiang, S. X. Liu, W. Y. Liang, S. J. Luo, Z. L. He, Y. Q. Ge, H. D. Wang, R. Cao, F. Zhang, Q. Wen, J. Q. Li, Q. L. Bao, D. Y. Fan, and H. Zhang, "Broadband nonlinear photonics in few-layer MXene $Ti_3C_2T_x$ (T=F, O, or OH)," Laser Photon. Rev. **12**, 1870013 (2018).
28. L. Lu, X. Tang, R. Cao, L. M. Wu, Z. J. Li, G. H. Jing, B. Q. Dong, S. B. Lu, Y. Li, Y. J. Xiang, J. Q. Li, D. Y. Fan, and H. Zhang, "Broadband nonlinear optical response in few-layer antimonene and antimonene quantum dots: a promising optical Kerr media with enhanced stability," Adv. Opt. Mater. **5**, 1700301 (2017).
29. H. Zhang, S. B. Lu, J. Zheng, J. Du, S. C. Wen, D. Y. Tang, and K. P. Loh, "Molybdenum disulfide (MoS_2) as a broadband saturable absorber for ultra-fast photonics," Opt. Express **22**, 7249–7260 (2014).
30. R. Wang, H. C. Chien, J. Kumar, N. Kumar, H. Y. Chiu, and H. Zhao, "Third-harmonic generation in ultrathin films of MoS_2," ACS Appl. Mater. Interfaces **6**, 314–318 (2013).
31. H. Y. Shi, R. S. Yan, S. Bertolazzi, J. Brivio, B. Gao, A. Kis, D. Jena, H. G. Xing, and L. B. Huang, "Exciton dynamics in suspended monolayer and few-layer MoS_2 2D crystals," ACS Nano **7**, 1072–1080 (2013).
32. K. F. Mak, C. Lee, J. Hone, J. Shan, and T. F. Heinz, "Atomically thin MoS_2: a new direct-gap semiconductor," Phys. Rev. Lett. **105**, 136805 (2010).
33. S. Wang, H. Yu, H. Zhang, A. Wang, M. Zhao, Y. Chen, L. Mei, and J. Wang, "Broadband few-layer MoS_2 saturable absorbers," Adv. Mater. **26**, 3538–3544 (2014).
34. K. Wang, J. Wang, J. Fan, M. Lotya, A. O'Neill, D. Fox, Y. Feng, X. Zhang, B. Jiang, Q. Zhao, H. Zhang, J. N. Coleman, L. Zhang, and W. J. Blau, "Ultrafast saturable absorption of two-dimensional MoS_2 nanosheets," ACS Nano **7**, 9260–9267 (2013).
35. R. Wang, B. A. Ruzicka, N. Kumar, M. Z. Bellus, H. Y. Chiu, and H. Zhao, "Ultrafast and spatially resolved studies of charge carriers in atomically thin molybdenum disulfide," Phys. Rev. B **86**, 045406 (2012).
36. Y. W. Song, S. Yamashita, C. S. Goh, and S. Y. Set, "Carbon nanotube mode lockers with enhanced nonlinearity via evanescent field interaction in D-shaped fibers," Opt. Lett. **32**, 148–150 (2007).
37. M. Nakazawa, S. Nakahara, T. Hirooka, M. Yoshida, T. Kaino, and K. Komatsu, "Polymer saturable absorber materials in the 1.5 micron band using poly-methyl-methacrylate and polystyrene with single-wall carbon nanotubes and their application to a femtosecond laser," Opt. Lett. **31**, 915–917 (2006).
38. V. Scardaci, Z. Sun, F. Wang, A. G. Rozhin, T. Hasan, F. Hennrich, I. H. White, W. I. Milne, and A. C. Ferrari, "Carbon nanotube polycarbonate composites for ultrafast lasers," Adv. Mater. **20**, 4040–4043 (2008).
39. N. Nishizawa, Y. Seno, K. Sumimura, Y. Sakakibara, E. Itoga, H. Kataura, and K. Itoh, "All-polarization-maintaining Er-doped ultrashort pulse fiber laser using carbon nanotube saturable absorber," Opt. Express **16**, 9429–9435 (2008).
40. S. Yamashita, A. Martinez, and B. Xu, "Short pulse fiber lasers mode-locked by carbon nanotubes and graphene," Opt. Fiber Technol. **20**, 702–713 (2014).
41. L. Li, S. Z. Jiang, Y. G. Wang, L. N. Duan, D. Mao, Z. Li, B. Y. Man, and J. H. Si, "WS_2/fluorine mica (FM) saturable absorbers for all-normal-dispersion mode-locked fiber laser," Opt. Express **23**, 28698–28706 (2015).
42. L. Li, Y. G. X. Wang, G. W. Yang, S. Z. Jiang, Z. Li, B. Y. Man, and Y. S. Wang, "Er-doped mode-locked fiber laser with WS_2/fluorine mica (FM) saturable absorber," Opt. Laser Technol. **90**, 109–112 (2017).
43. L. H. Huo, W. Li, L. H. Lu, H. N. Cui, S. Q. Xi, J. Wang, B. Zhao, Y. C. Shen, and Z. H. Lu, "Preparation, structure and properties of three-dimensional ordered α-Fe_2O_3 nanoparticulate film," Chem. Mater. **12**, 790–794 (2000).
44. M. Clemente-León, T. Ito, H. Yashiro, and T. Yamase, "Two-dimensional array of polyoxomolybdate nanoball constructed by Langmuir-Blodgett semiamphiphilic method," Chem. Mater. **19**, 2589–2594 (2007).
45. H. Zhu, B. Akkus, Y. Gao, Y. Liu, S. Yamamoto, J. Matsui, T. Miyashita, and M. Mitsuishi, "Regioselective synthesis of eight-armed cyclosiloxane amphiphile for functional 2D and 3D assembly motifs," ACS Appl. Mater. Interfaces **9**, 28144–28150 (2017).
46. P. G. Yan, Z. K. Jiang, H. Chen, J. D. Yin, J. T. Lai, J. Z. Wang, T. H. He, and J. B. Yang, "α-In_2Se_3 wideband optical modulator for pulsed fiber lasers," Opt. Lett. **43**, 4417–4420 (2018).
47. J. T. Wang, H. Chen, Z. K. Jiang, J. D. Yin, J. Z. Wang, M. Zhang, T. H. He, J. Z. Li, P. G. Yan, and S. C. Ruan, "Mode-locked thulium-doped fiber laser with chemical vapor deposited molybdenum ditelluride," Opt. Lett. **43**, 1998–2001 (2018).
48. M. Michiaki, K. Shinnen, I. Shinzaburo, Y. Masahide, S. Albert, and K. Wolfgang, "Preparation and characterization of the Langmuir-Blodgett films made of hairy-rod polyglutamates bearing various chromophores in the side chain," Langmuir **14**, 7260–7266 (1998).
49. Z. K. Wu, S. X. Wu, and Y. Q. Liang, "Monolayer behavior and LB film structure of poly(2-methoxy-5-(n-hexadecyloxy)-p-phenylene vinylene)," Langmuir **17**, 7267–7273 (2001).
50. H. Li, Q. Zhang, C. C. R. Yap, B. K. Tay, T. H. T. Edwin, A. Olivier, and D. Baillargeat, "From bulk to monolayer MoS_2: evolution of Raman scattering," Adv. Funct. Mater. **22**, 1385–1390 (2012).
51. J. T. Wang, Z. K. Jiang, H. Chen, J. R. Li, J. D. Yin, J. Z. Wang, T. H. He, P. G. Yan, and S. C. Ruan, "High energy soliton pulse generation by a magnetron-sputtering-deposition-grown $MoTe_2$ saturable absorber," Photon. Res. **6**, 535–541 (2018).
52. D. Tang, W. Man, H. Tam, and P. Drummond, "Observation of bound states of solitons in a passively mode-locked fiber laser," Phys. Rev. A **64**, 033814 (2001).
53. Y. D. Wang, D. Mao, X. T. Gan, L. Han, C. J. Ma, T. L. Xi, X. Zhang, W. Y. Shang, S. J. Hua, and J. L. Zhao, "Harmonic mode locking of bound-state solitons fiber laser based on MoS_2 saturable absorber," Opt. Express **23**, 205–210 (2015).
54. M. Chernysheva, A. Bednyakova, M. A. Araimi, R. C. T. Howe, G. H. Hu, T. Hasan, A. Gambetta, G. Galzerano, M. Rümmeli, and A. Rozhin, "Double-Wall carbon nanotube hybrid mode-locker in Tm-doped fibre laser: a novel mechanism for robust bound-state solitons generation," Sci. Rep. **7**, 44314 (2017).
55. N. H. Seong and D. Y. Kim, "Experimental observation of stable bound solitons in a figure-eight fiber laser," Opt. Lett. **27**, 1321–1323 (2002).
56. E. Yoshida and M. Nakazawa, "80~200 GHz erbium doped fibre laser using a rational harmonic mode-locking technique," Electron. Lett. **32**, 1370–1372 (1996).